



## Effect of inorganic ions on the photocatalytic treatment of methylene blue by reduced graphene oxide

Dan Li<sup>a</sup>, Heng Liu<sup>a</sup>, Wei Peng<sup>b</sup>, Feigao Xu<sup>c,\*</sup>

<sup>a</sup>School of Resources, Environmental and Chemical Engineering, Nanchang University, 999 Xuefu Avenue, Nanchang 330031, China, Tel. +86 791 86763662; email: 13122568@qq.com (D. Li), Tel. +86 791 86763662; email: 1125066427@qq.com (H. Liu)

<sup>b</sup>Laboratory of Environmental Sanitary and Engineering, Department of Industrial Engineering, Padova University, Lungargine G. Rovetta 8, Padova 35127, Italy, email: 827388687@qq.com

<sup>c</sup>College of Chemistry, Nanchang University, 999 Xuefu Avenue, Nanchang 330031, China, Tel./Fax: 86 791 86763662; email: xufeigao@ncu.edu.cn

Received 30 May 2018; Accepted 28 November 2018

### ABSTRACT

In this study, reduced graphene oxide (RGO) was prepared separately by hydrothermal and chemical reduction methods. The catalytic activity of RGO with hydrothermal and the chemical methods was investigated when they were applied in the degradation of methylene blue (MB) under visible light. The results show that the catalytic activity of RGO with the chemical method was negligible, whereas that of RGO with the hydrothermal method was significant but unstable. The addition of 2 mmol L<sup>-1</sup> inorganic ions (HCO<sub>3</sub><sup>-</sup>, HPO<sub>4</sub><sup>2-</sup>, NO<sub>3</sub><sup>-</sup>, SO<sub>4</sub><sup>2-</sup>, Al<sup>3+</sup>, Mg<sup>2+</sup>, Na<sup>+</sup>, Ca<sup>2+</sup>, and NH<sub>4</sub><sup>+</sup>) and humic acid (HA) into RGO with the hydrothermal method affected the degradation of MB. The photodegradation efficiency of MB was improved by the addition of HCO<sub>3</sub><sup>-</sup> or HPO<sub>4</sub><sup>2-</sup>, whereas NO<sub>3</sub><sup>-</sup>, SO<sub>4</sub><sup>2-</sup>, Al<sup>3+</sup>, Mg<sup>2+</sup>, Na<sup>+</sup>, Ca<sup>2+</sup>, and NH<sub>4</sub><sup>+</sup> inhibited photodegradation of MB. Moreover, the addition of HA was proven to inhibit the degradation of MB by RGO via the hydrothermal method.

*Keywords:* Reduced graphene oxide; Hydrothermal reduction; Photocatalysis

### 1. Introduction

Organic dyes are the major pollutants in wastewaters originating from the textile chemical industry [1,2]. Organic dyes are not only generally resistant to microbial degradation but also easily converted into toxic or carcinogenic substances [3]. At present, a number of methods such as electrolyte decomposition, chemical precipitation, ion exchange, adsorption, sedimentation, etc. have been used for the removal of organic dyes [4–8]. However, the aforementioned techniques have certain drawbacks including a slow rate of dye removal, high cost, regeneration, time consumption, difficult disposal, etc.

Heterogeneous photocatalysis has been proven as an effective treating method for the purification of dye-containing

wastewater [9,10]. Textile wastewaters usually contain various inorganic ions that originate from different printing and dyeing processes [11–14]. It is notable that inorganic ions might influence the photocatalytic reactions when treating textile wastewaters with the photocatalytic oxidation method. The effect of inorganic ions on degradation of dye in TiO<sub>2</sub> dispersions under ultraviolet ray irradiation has been reported [14–17].

Recently, graphene, an atomic-layer-thick two-dimensional carbon nanostructure, has attracted tremendous research interests [18–20], due to its outstanding electronic, optical, thermal, and mechanical properties and theoretically high surface area of ~2,600 m<sup>2</sup>·g<sup>-1</sup>. Therefore, graphene has shown a variety of applications in nanoelectronics, sensors, batteries, supercapacitors, and catalysis [20]. Furthermore, it is

\* Corresponding author.

remarkable that pristine graphene is a zero-band gap semiconductor and possesses a superior electrical conductivity in accepting and transporting electrons to its analogies such as carbon nanotubes [21]. Graphene has a very high chemical reactivity. Gao et al. [22] observed that graphene can catalyse the hydrogenation of nitrobenzene with very high efficiency even at room temperature.

So far, various methods have been developed to restore the graphene prepared with graphene oxide (GO), which include chemical reduction method [23], electrochemical reduction [24], hydrothermal dehydration [25], etc. Khalid et al. [26], and Zhang et al. [27] demonstrated a simple hydrothermal method to prepare TiO<sub>2</sub>-graphene (TiO<sub>2</sub>-reduced graphene oxide [RGO]) composites. The prepared TiO<sub>2</sub>-RGO composites showed not only an extended light absorption range but also a higher photocatalytic activity for the degradation of methyl orange under visible light irradiation. Min and Lu [28] synthesised the photocatalyst for degrading the dye Eosin Y by sensitising RGO with dispersed Pt nanoparticles, and it exhibited high photocatalysis activity for hydrogen evolution from water reduction under visible light irradiation ( $\lambda \geq 420$  nm). However, the effects of the types of inorganic ions on the photocatalytic activity of RGO under visible light irradiation have not been reported.

Hydrothermal and chemical reduction methods are both methods of the preparation of graphene. The chemical reduction method is currently one of the most widely used methods for the preparation of graphene by RGO. It mainly utilises hydrazine hydrate to remove oxygen-containing functional groups on the surface of GO. The hydrothermal method utilises the high temperature and high pressure hydrothermal or solvothermal conditions to rapidly decompose a large amount of oxygen-containing functional groups between the GO layers to generate a large amount of gas.

In this paper, RGO was prepared using hydrothermal and chemical reduction methods, respectively, and their catalytic activities were evaluated. Six different types of inorganic ions (Cl<sup>-</sup>, SO<sub>4</sub><sup>2-</sup>, NO<sub>3</sub><sup>-</sup>, H<sub>2</sub>PO<sub>4</sub><sup>-</sup>, Ca<sup>2+</sup>, and Mg<sup>2+</sup>) and humic acid (HA), which are common in synthetic dye-containing effluent, were chosen to investigate the effects of their addition on the photodegradation of methylene blue (MB) in RGO aqueous dispersions under visible light irradiation.

## 2. Experimental procedure

### 2.1. Materials

Graphite powder (99.95%, 325 mesh) was purchased from Nanjing Xianfeng Chemical Reagent Corporation, Nanjing, China. MB was obtained commercially from the Sinopharm Chemical Reagent Corporation and used as received. Inorganic salts, Na<sub>2</sub>HPO<sub>4</sub>, NaHCO<sub>3</sub>, NaNO<sub>3</sub>, Na<sub>2</sub>SO<sub>4</sub>, NaCl, (NH<sub>4</sub>)<sub>2</sub>SO<sub>4</sub>, MgSO<sub>4</sub> and Al<sub>2</sub>(SO<sub>4</sub>)<sub>3</sub>·18H<sub>2</sub>O served as the sources of ions, and they were supplied by the Sinopharm Chemical Reagent Corporation, Shanghai, China. Glass fibre filter paper was purchased from Shanghai Bangwo Instrument Equipment Co., Ltd., Shanghai, China. The HA sample was obtained from the Shanghai Aladdin Chemical Reagent Corporation, China. Ultrapure water (resistivity  $\geq 18$  M $\Omega$ ·cm) was used during the experimental process.

### 2.2. Preparation of purified HA solution

The preparation method of the purified HA sample was as follows [29]: to remove impurities, 0.1 mol L<sup>-1</sup> HCl solution was added into the HA solution at a liquid to solid ratio (L/S) = 1/20. The mixture was centrifuged at 4,000 rpm for 60 min. After centrifugation, the supernatant was withdrawn. The concentrated HA was washed with ultrapure water until the pH of the eluate was neutral. Next, the treated HA mixed with 200 mL deionised water was rotated at 4,000 rpm for 60 min. After centrifugation, the supernatant was withdrawn again. The treated HA was mixed with 0.1 mol L<sup>-1</sup> NaOH and then filtered through glass fibre filter paper. The HA filtrate was dried at 60°C. A stock solution of HA with 1,000 mg L<sup>-1</sup> was prepared.

### 2.3. Preparation of RGO-C and RGO-H

GO was prepared from natural graphite using the modified Hummers method [30,31]. Three grams of graphite was added into a mixture of 12 mL of concentrated H<sub>2</sub>SO<sub>4</sub>, 2.5 g of P<sub>2</sub>O<sub>5</sub>, and 2.5 g of K<sub>2</sub>S<sub>2</sub>O<sub>8</sub>. The solution was heated to 80°C and kept stirring for 5 h in a water bath. Then, the mixture was diluted with 500 mL of deionised water, and the product was obtained by filtering using a 0.2- $\mu$ m nylon film and dried under ambient conditions. Then, the product was reoxidised by the Hummers and Offeman methods to produce the graphite oxide [27]. After exfoliation by sonicating 1 mg mL<sup>-1</sup> of graphite oxide dispersion for 1 h, the GO was recovered by filtration and vacuum drying.

RGO-H was prepared by the hydrothermal method [32]. In a typical synthetic procedure, 100 mL GO was treated with the ultrasound (25 kHz, 700 W) for 1.5 h and then was maintained at 180°C for 12 h in a blast oven to simultaneously achieve the reduction of GO. Afterwards, the obtained dispersions were filtered and then washed with deionised water three times. Finally, they were placed into a vacuum drying oven in 60°C. RGO-C was prepared by the chemical reduction method [33]. GO in ultrapure water (100 mL) was treated with ultrasound sonication for 1.5 h. Then hydrazine hydrate (1 mL) was added to the mixture solution at 100°C for 24 h. The resulting RGO-C was washed with ultrapure water by centrifugation.

### 2.4. Photocatalytic experiments

An aqueous solution of the MB dyes (20 mg L<sup>-1</sup>, 100 mL) and the 100 mg of RGO-C or RGO-H were mixed and stirred in a 100-mL cylindrical beaker under ambient conditions (25°C $\pm$ 1°C). Meanwhile, the photoreaction vessels were exposed to the UV irradiation produced by a 500 W Xe lamp. The visible source was provided by inserting a cut-off filter behind the lamp for absorbing UV irradiation, and this visible source covered the wavelengths of range 400–700 nm. The light intensity at the catalyst mixture surface was estimated to be 177 W m<sup>-2</sup> with a radiometer. The lamp was surrounded by a circulating water jacket so that the temperature in the reactor could remain constant.

In the RGO system, an aqueous RGO dispersion was prepared by adding 100 mg of RGO powder to a 100 mL of solution containing MB and inorganic anions at designed concentrations of 20 mg L<sup>-1</sup>. Prior to irradiation, the dispersions

were magnetically stirred under dark conditions for 60 min to achieve the adsorption equilibrium of MB by the catalyst. The equilibrium concentration of MB was used as the initial value of the further kinetic calculation of the photodegradation process. All irradiation experiments were conducted under continuous stirring. 2-mL samples were withdrawn for UV–Vis analysis at regular time intervals and filtered by syringe filtration through NAVIGATOR Nylon Millipore filters (0.22  $\mu\text{m}$ ). The concentrations of MB in each treated sample were determined spectrophotometrically (Beijing Ordinary General Instrument Co., Ltd., Beijing, China) at  $\lambda_{\text{max}} = 642 \text{ nm}$ .

### 2.5. Stability of the photocatalyst

It is well known that stability is a key consideration for evaluating the practical application of the photocatalyst. To investigate the stability of RGO, the photocatalyst was recycled for MB degradation under visible light. The experiment comprises the following steps: first, MB was absorbed by the catalyst for 60 min, followed by degradation of MB with the catalyst for 50 min. After washing with pure water, the recovered catalyst was reused for the next cycle. Five cycles were completed in the experiments.

### 2.6. Analytical method

The chemical bonds of the materials synthesised were analysed by Fourier-transform infrared spectrophotometry (FTIR). The spectra of the powders extracted from the samples were recorded using a Nicolet Nexus 870 FTIR spectrometer in the region from 4,000 to 400  $\text{cm}^{-1}$ .

Samples were also characterised for thermal behaviour using simultaneous differential thermal analysis (TA-SDT600), with a heating rate of 10°C·min<sup>-1</sup> to 800°C. The instrument was purged with N<sub>2</sub> at a flow rate of 100 mL·min<sup>-1</sup>.

A palladium–gold alloy was vacuum evaporated onto RGO-H, RGO-C, and GO, respectively. Then the outer surfaces of these samples were studied using a ZEISS EVO18 (Jena, Germany) scanning electronic microscope (SEM) at 3 kV of accelerating voltage under various magnifications.

The high resolution transmission electron microscope (HRTEM) and selected area electron diffraction (SAED) patterns were examined with a JEM-2100 (JEOL, Japan) microscope equipped with a field-emission electron gun and operating at 200 kV. For that, selected samples were dispersed in a water suspension, and a drop of the suspension was placed over a grid with porous carbon film.

The textural properties of the RGO-H and RGO-C samples were characterised by N<sub>2</sub> adsorption–desorption isotherms at 77 K on a JW-K adsorption analyser (Jinweigaobo Instrument Corp, Beijing). The samples were outgassed under high vacuum for 5 h at 200°C. The specific surface area was calculated by the Brunner–Emmet–Teller (BET) method.

## 3. Results and discussion

### 3.1. Characterisation of RGO-H, RGO-C, and GO

The SEM images of the GO, RGO-H, and RGO-C samples are shown in Fig. 1. It can be seen that GO showed a lamellar structure, and its surface is relatively smooth, whereas the RGO-H material consists of randomly aggregated, crumpled

sheets closely associated with each other and forming a disordered structure. For RGO-C, it has a two-dimensional planar sheet structure of many folds. It is worth noting that the crumpled three-dimensional structure of the sheets still leaves many exposed surfaces.

The transmission electron microscope (TEM) images of GO and RGO along with SAED are shown in Fig. 2. The micrographs of GO and RGO display typical transparent morphology and a rippled surface. This may be part of their intrinsic nature, which can be attributed to the 2D membrane structure becoming thermodynamically stable via rippling. From the SAED patterns depicted in the inset, it is clear that the diffraction spots are ringlike, suggesting that the crystal structures of GO and RGO are destroyed during oxidation–reduction.

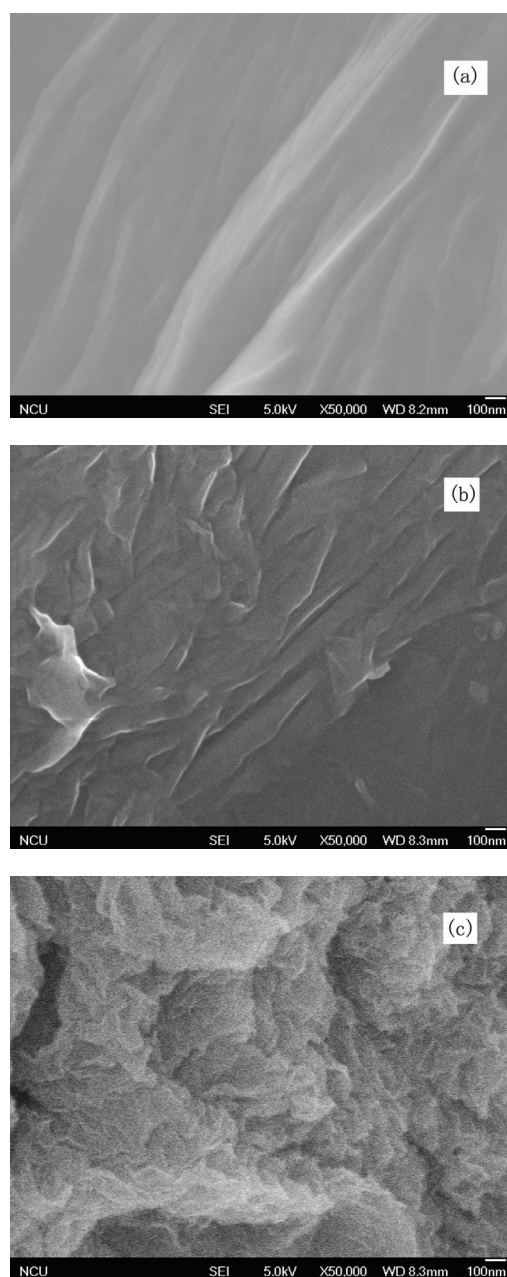


Fig. 1. SEM image of (a) GO, (b) RGO-H, and (c) RGO-C ( $\times 50,000$ ).

The FTIR spectra (Fig. 3) also showed that the RGO-H contained some oxygen functional groups compared with GO. The absorption band appearing ca.  $1,600\text{ cm}^{-1}$  clearly showed the skeletal vibration of the graphene sheets, indicating the formation of graphene during the hydrothermal reaction. This skeletal vibration peak was also observed in the FTIR spectrum of graphene prepared by the hydrothermal reduction of GO. In addition, in Fig. 3, the small peak approximately  $1,726\text{ cm}^{-1}$  was assigned to the C=O stretching of the residual COOH groups [26], whereas RGO-C had no oxygen functional groups.

The TGA analysis of GO, RGO-C, and RGO-H is shown Fig. S1. GO was thermally unstable and starts to lose mass upon heating even below  $100^\circ\text{C}$ , and the major mass loss occurs between  $200^\circ\text{C}$  and  $300^\circ\text{C}$ . This weight loss was presumably due to the pyrolysis of the labile oxygen-containing functional groups, yielding water vapour,  $\text{CO}_2$ , and CO [34,35]. On the other hand, the removal of the thermally labile oxygen functional groups results in greatly increased thermal stability for the RGO-C compared with RGO-H. Apart from a slight loss of mass below  $100^\circ\text{C}$ , which can be attributed to the loss of adsorbed water, no significant mass loss was detected when RGO-C was heated up to  $800^\circ\text{C}$ . On the

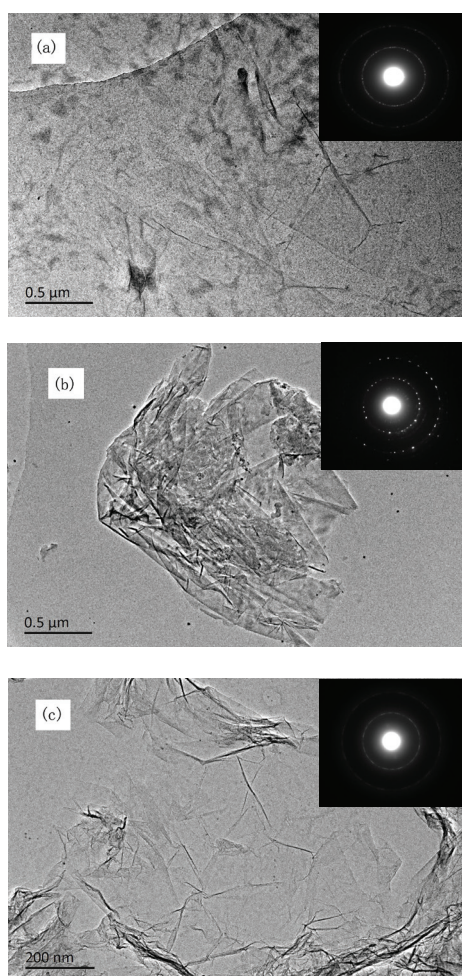


Fig. 2. TEM image and SAED patterns of (a) GO, (b) RGO-H, and (c) RGO-C.

whole, the ignition loss of GO was the smallest, followed by RGO-H among GO, RGO-C, and RGO-H, and this was because RGO-H had more oxygen functional groups than RGO-C; this was consistent with the FTIR analysis, demonstrating the unsuccessful physical reduction of GO.

The surface area measurement of the RGO-C and RGO-H via adsorption–desorption (Fig. S2) yielded a BET value of  $242$  and  $63\text{ g m}^{-2}$ , respectively. The high specific surface area was partially an indication of the degree of GO exfoliation prior to the reduction. However, the experimental data were much lower than that of the production ( $466\text{ m}^2\text{ g}^{-1}$ ) prepared by Stankovich et al. [33] and the theoretical specific surface area for completely exfoliated and isolated graphene sheets ( $2,620\text{ m}^2\text{ g}^{-1}$ ) [36]. The reason was that GO was not completely exfoliated but rather agglomerated due to van der Waals attractive interaction during the preparation process. Meanwhile, this agglomeration will lead to the partial overlapping and coalescing of the reduced sheets, contributing to the decrease in the surface area of the bulk materials.

### 3.2. Photodegradation of MB with RGO-H and RGO-C as catalysts

RGO-H and RGO-C were added to the  $100\text{ mL}$  MB solution with the initial concentration of  $20\text{ mg L}^{-1}$ , respectively. As shown in Fig. 4, after adsorption in the dark for  $40\text{ min}$ , the reaction systems reached equilibrium for both RGO-H and RGO-C. The adsorption efficiencies at equilibrium for RGO-C and RGO-H were  $97\%$  and  $67\%$ , respectively. The comparatively higher adsorption capacity of RGO-C can be explained by the higher surface area of RGO-C compared with that of RGO-H. After the adsorption reached equilibrium, MB could be further removed by photodegradation of RGO-H while the photodegradation ability of RGO-C was negligible. Gao et al. [22] suggest that the unsaturated carbon atoms at the edges of RGO and defects on RGO may be catalytically active centres for organic material. The zigzag edges of RGO may act as catalytic active sites to facilitate the activation of a reactant molecule. Therefore, the catalytic activity of RGO-H is larger than that of RGO-C because RGO-H has more defects than RGO-C.

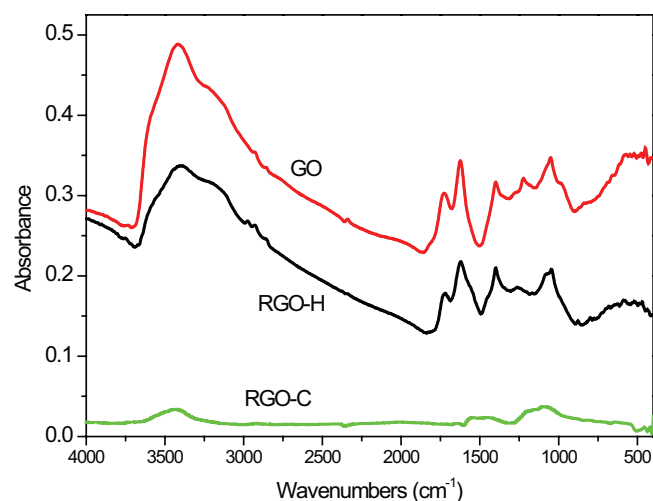


Fig. 3. FTIR spectra of GO, RGO-H, and RGO-C.

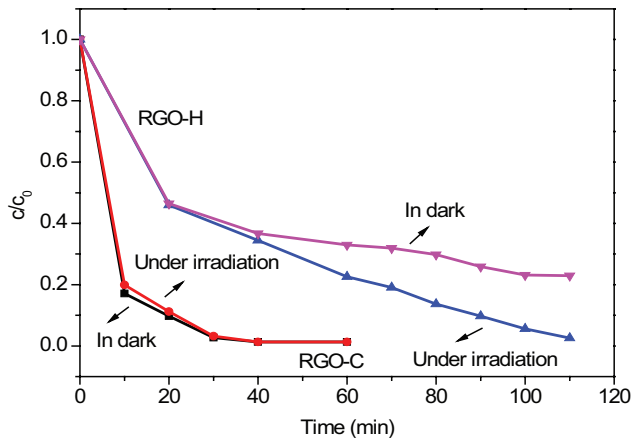


Fig. 4. Effect of MB degradation with RGO-H and RGO-C as photocatalysts.

### 3.3. Photocatalytic degradation of MB was conducted at different concentrations

The concentration of pollutants is a significant factor for photocatalytic processes. The photocatalytic degradation of MB was conducted at different concentrations (10, 20, 30, 40, and 50 mg L<sup>-1</sup>). The photocatalysis processes were evaluated by the pseudo-first-order kinetics expressed as follows:

$$-\ln(C/C_0) = kt \quad (1)$$

where  $C$  was the concentration of MB in each time period, and  $C_0$  was the concentration of MB after dark adsorption-desorption equilibrium.

According to Eq. (1), linear plots of  $\ln C/C_0$  vs. time are expected (see Fig. S3) from which slope  $k$  can be evaluated corresponding to different concentrations of MB. The  $k$  values are presented in Table S1. Notably the value of  $k$  decreased with the increase in MB concentration, indicating that the degradation efficiency was hindered. A possible reason for this could be that as the concentration of MB was increased, more MB molecules were adsorbed onto the surface of the catalyst. However, the MB molecules adsorbed onto the surface of the catalyst could not degrade immediately due to less penetration of the visible light. In other words, with the increase in MB concentration, fewer photons could arrive on the catalyst surface because of the more deeply coloured solution, followed by limiting or reducing the reactive radicals produced from the catalytic process. Therefore, an excessive concentration of pollutants will reduce the role of photocatalytic processes in water treatment.

### 3.4. Effect of inorganic anions on the photodegradation of MB

Considering the relatively higher catalytic activity of RGO-H, RGO-H was selected as the catalyst to evaluate the effects of inorganic anions on the photodegradation of MB.

#### 3.4.1. Effect of Cl<sup>-</sup> on the photodegradation of MB

The effect of Cl<sup>-</sup> on the photodegradation of MB under visible light irradiation was investigated by adding NaCl to the solution (Fig. 5). Clearly, Cl<sup>-</sup> enhances both the adsorption

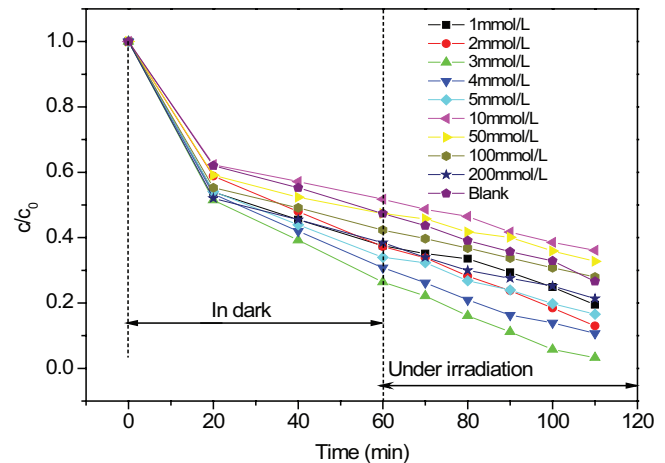
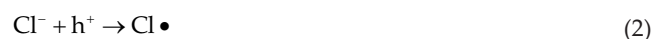


Fig. 5. The effect of Cl<sup>-</sup> on the photodegradation of MB.

and photodegradation rate of MB in the presence of a catalyst when the Cl<sup>-</sup> concentration ranges from 3 to 5 mmol L<sup>-1</sup>. However, when the Cl<sup>-</sup> concentration ranges from 10 to 200 mmol L<sup>-1</sup>, the adsorption and photodegradation rate of MB by the catalyst is suppressed. It can be concluded that when the chloride ion concentration is low, Cl<sup>-</sup> will capture OH•, making the hole shrink and suppress the light pair, which in turn inhibits the adsorption of MB onto the RGO surface. That is why the chloride ion increases the photocatalytic degradation of MB by RGO-H.

On the other hand, when the chloride ion concentration is high, competitive adsorption is inevitable because MB is an anionic dye. As a result, in the RGO-H system, the observed inhibition effect can be explained by competitive adsorption [37]. Another reason maybe that chloride ions can act as scavengers of OH• radicals. Several studies have reported that chloride ions can scavenge h<sup>+</sup> and •OH by the following general reactions [38–40]:



These radicals can be reduced back to chloride ions by electrons and therefore reduce the availability of holes, electrons, and OH•. On the basis of the provided results, it can be suggested that the appreciable level of salts in practical wastewater may adversely affect the efficiency of the removal of pollutants.

The semi-logarithmic graph of  $(C/C_0)$  is shown in Fig. S4 under different Cl<sup>-</sup> concentration as a function of time. As shown, the degradation rate constants under different Cl<sup>-</sup> concentrations were consistent with pseudo-first-order kinetics. The pseudo-first-order kinetics can be expressed as follows:

$$\ln \frac{C_0}{C} = kt \quad (6)$$

where  $C_0$  and  $C$  are the reactant concentrations at time  $t = 0$  and  $t = t$ , respectively;  $K$  and  $t$  are the degradation rate constant and time, respectively.

A plot of  $-\ln(C_0/C)$  vs.  $t$  will yield a slope of  $K$ . As the  $\text{Cl}^-$  concentration increased from 0 to 3 mmol  $\text{L}^{-1}$ , the value of  $K$  increased from 0.01092 to 0.04249  $\text{min}^{-1}$ . Based on the theory of Eq. (6), it is possible that trace amounts of chloride are prone to capturing hydroxyl radicals, whereas the competitive adsorption of chloride is not obvious. When the concentration of  $\text{Cl}^-$  ranged from 3–5 mmol  $\text{L}^{-1}$ , the value of  $K$  decreased from 0.04249 to 0.01475  $\text{min}^{-1}$ , but the value was still higher compared with that of group under the condition of no chloride (0.01092  $\text{min}^{-1}$ ). Therefore, it can be concluded that the higher the chloride ion concentration, the greater the influence of the chloride ion concentration on competitive adsorption. The value of  $K$  was 0.00745, 0.00745, 0.00832, and 0.0112  $\text{min}^{-1}$  when the  $\text{Cl}^-$  concentration was 10, 50, 100, and 200 mmol  $\text{L}^{-1}$ , respectively. The results suggest that the competitive adsorption of chloride onto the catalyst seriously inhibits the photocatalytic degradation efficiency of MB.

### 3.4.2. Effect of $\text{SO}_4^{2-}$ , $\text{NO}_3^-$ , $\text{HCO}_3^-$ , and $\text{HPO}_4^{2-}$ on the photodegradation of MB

To compare the effects of different anions on the photodegradation of MB, we used the same concentration for anions (2 mmol  $\text{L}^{-1}$ ). The effects of different anions on the photodegradation of MB under visible light irradiation are depicted in Fig. 6. All anions showed inhibition effects on adsorption of RGO-H.

Anions, such as  $\text{SO}_4^{2-}$ ,  $\text{NO}_3^-$ , and  $\text{Cl}^-$  could be adsorbed onto the surface of RGO-H in acidic conditions due to electrostatic attraction. Among the three anions mentioned,  $\text{NO}_3^-$  showed the strongest inhibitory effect on the adsorption of MB. The addition of anions played two roles in the photodegradation of the selected dyes. The first was that anions affected the MB degradation by changing the surface charge

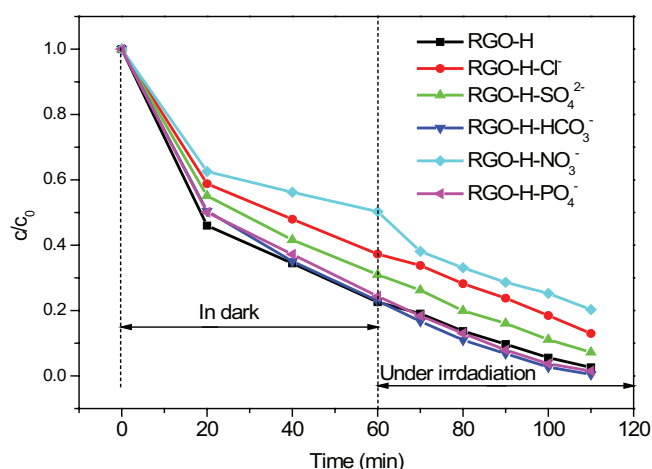


Fig. 6. The photodegradation of MB for RGO-H in different anions.

of RGO, resulting in a change in the distribution of dye molecules between the solution and the RGO surface. Another pathway was that the adsorbed anions such as  $\text{SO}_4^{2-}$  reacted with the positive holes ( $\text{h}^+$ ) and hydroxyl radicals ( $\text{OH}\cdot$ ), as shown in Eqs. (7) and (8):



It is well known that  $\text{SO}_4^{\cdot -}$  is less reactive than  $\text{OH}\cdot$  and  $\text{h}^+$ ; therefore, the excess  $\text{SO}_4^{2-}$  will hinder the photocatalytic decolourisation of the selected dyes.

Under visible light irradiation,  $\text{Cl}^-$ ,  $\text{SO}_4^{2-}$ , and  $\text{NO}_3^-$  can inhibit the photodegradation of the dye while  $\text{HCO}_3^-$  and  $\text{HPO}_4^{2-}$  can improve the photodegradation of the dye. This study demonstrated that different anions had different effects on the photodegradation of MB. In addition to this, the inhibitory effect of anions on the photodegradation of MB was due to competitive adsorption.

### 3.5. Effects of inorganic cations on the photodegradation of MB

The effects of different cations on the photodegradation of MB under visible light irradiation are shown in Fig. 7. As can be noticed, under visible light irradiation,  $\text{Ca}^{2+}$ ,  $\text{Mg}^{2+}$ ,  $\text{NH}_4^+$ , and  $\text{Al}^{3+}$  can inhibit the photodegradation of the dye.

On the one hand,  $\text{Al}^{3+}$  has a relatively higher charge compared with  $\text{Ca}^{2+}$  and  $\text{Mg}^{2+}$ . The addition of cation increases the ionic strength, thereby suppressing the compression electric double layer according to electrostatic repulsion theory. Compared with other cations,  $\text{Al}^{3+}$  can be added to improve the photocatalytic degradation efficiency of MB. The reason is because the ionic strength of  $\text{Al}^{3+}$  is the highest among the cations, and this can be attributed to the effective function between the cations and the strong electrostatic region in the compressed electric double layer. On the other hand, all three cations,  $\text{Ca}^{2+}$ ,  $\text{Mg}^{2+}$ , and  $\text{NH}_4^+$ , can capture electrons, which will inhibit the recombination of the photogenerated

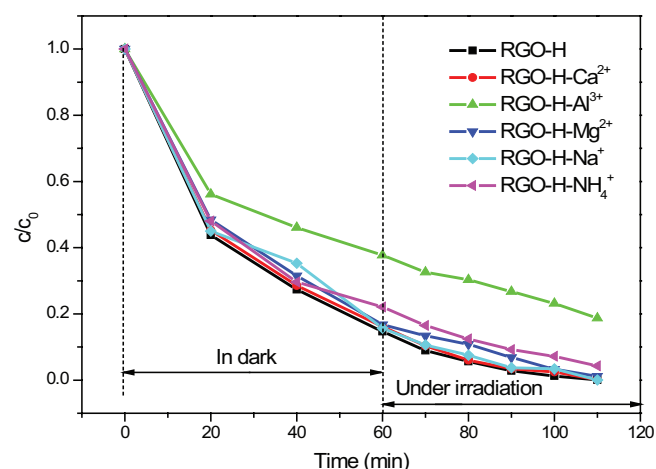


Fig. 7. The photodegradation of MB for RGO-H in different cations.

electron–hole pair, decreasing the photocatalytic degradation efficiency. In addition, the effect of  $Mg^{2+}$  on RGO adsorption is stronger than that of  $NH_4^+$ ; overall, the inhibitory effects of inorganic cations on the photodegradation of MB follow the sequence  $Al^{3+} > NH_4^+ > Mg^{2+} > Na^+ > Ca^{2+}$ .

### 3.6. Effect of HA on the photodegradation of MB

HA is the most abundant organic acid in the environment, and it is widely found in water, lacustrine and marine sediments, and soil organic matter [41,42]. HA is a type of natural organic mixture, and its chemical structure is complex, with carboxyl, phenolic, ketone, and other active groups. The effect of HA on the photocatalytic degradation rate is investigated in Fig. 8. The results showed that the amount of adsorption of MB increased with the addition of HA. The adsorption rates of RGO, HA, and RGO/HA were 39%, 36%, and 61%, respectively. When the HA was added into the graphene system, the degradation rate of MB also decreased. The photodegradation rates of MB by RGO and RGO/HA were 10% and 8%, respectively, after being irradiated for 60 min under visible light. The inhibitory effect of HA on the photocatalytic degradation of MB could be attributed to photocatalyst deactivation and  $OH\cdot$  scavenging. However, scholars have argued

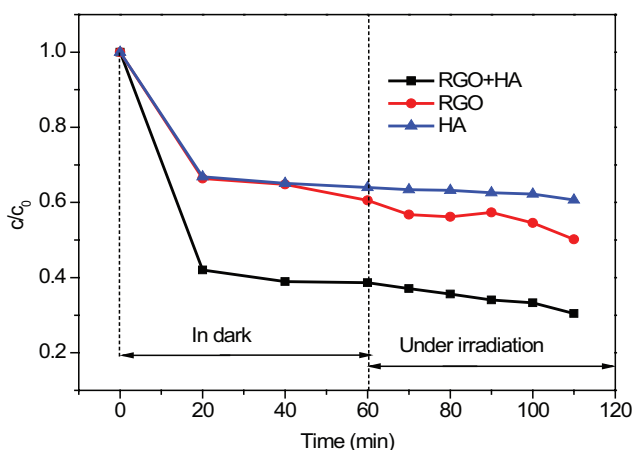


Fig. 8. Effect of HA on the RGO-H photocatalytic degradation of MB.

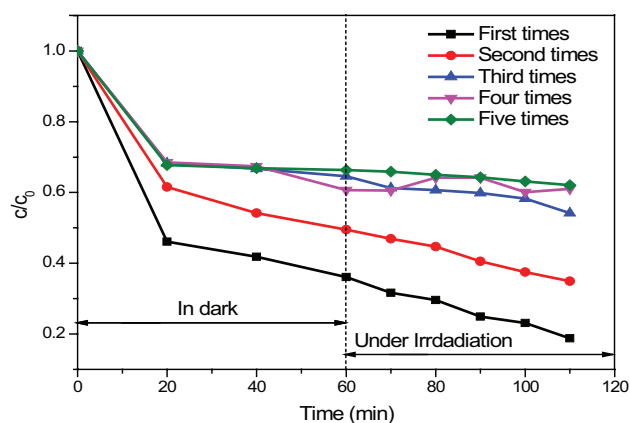


Fig. 9. Influence of long-term use on the efficiency of RGO-H.

that HA can improve the photocatalytic degradation ability of  $TiO_2$  [43]. Nevertheless, more studies are needed to clarify the contribution of inhibitory mechanisms.

### 3.7. Stability of the photocatalyst

The efficiency of the catalyst showed a significant decrease after five consecutive experiments (Fig. 9). The results indicated that the stability of the RGO-H prepared by the hydrothermal method was poor. At the same time, the adsorption process was also repeated five times for comparison. After the reaction system reached adsorption equilibrium, the catalyst was reused directly without any photocatalytic reaction. It can be seen that the reused catalyst had small adsorption ability for MB. However, the photocatalytic activity of the catalyst decreased significantly after five consecutive recycle experiments, implying that the MB adsorbed onto the catalyst degraded little during the photocatalytic progress.

## 4. Conclusions

Two RGOs, RGO-H and RGO-C, were prepared by hydrothermal and chemical reduction methods, respectively. The catalytic activity of RGO-C and RGO-H was investigated when they were applied in the degradation of MB under visible light. The results of this study indicate that the structure and catalytic activity of RGO-C and RGO-H were different. The catalytic activity of RGO-C was negligible, whereas that of RGO-H was very high but unstable. In addition, the presence of various inorganic ions such as  $SO_4^{2-}$ ,  $NO_3^-$ ,  $Mg^{2+}$ ,  $Ca^{2+}$ ,  $NH_4^+$ , and  $Al^{3+}$  inhibited the photodegradation of the dye while  $HCO_3^-$  and  $HPO_4^{2-}$  improved the photodegradation of MB. HA inhibited the degradation of MB by RGO-H.

## Acknowledgements

The work was supported by State Key Laboratory of Pollution Control and Resource Reuse open foundation for financial support under research projects PCRRF11018, and Foundation of the Creative Experimental Project of National undergraduate students for financial support under research projects 20140403029.

## References

- [1] A. Keck, J. Klein, M. Kudlich, A. Stolz, H.J. Knachmuss, R. Mattes, Reduction of azo dyes by redox mediators originating in the naphthalenesulfonic acid degradation pathway of *Sphingomonas* sp. strain BN6, *Appl. Environ. Microbiol.*, 63 (1997) 3684–3690.
- [2] A.M.T. Mata, A. Ligneul, N. Lourençoc, H.M. Pinheiro, Advanced oxidation for aromatic amine mineralization after aerobic granular sludge treatment of an azo dye containing wastewater, *Desal. Water Treat.*, 91 (2017) 168–174.
- [3] F. Xu, W. Tan, H. Liu, D. Li, Y. Li, M. Wang, Immobilization of PDMS-SiO<sub>2</sub>-TiO<sub>2</sub> composite for the photocatalytic degradation of dye AO-7, *Water Sci. Technol.*, 74 (2016) 1680–1688.
- [4] W. Wang, M. Yang, Y. Ku, Photoelectrocatalytic decomposition of dye in aqueous solution using Nafion as an electrolyte, *Chem. Eng. J.*, 165 (2010) 273–280.
- [5] R.G. Jenita, R.M.A. Jothi, K.G. Gnana, Reduced graphene oxide/ZnFe<sub>2</sub>O<sub>4</sub> nanocomposite as an efficient catalyst for the photocatalytic degradation of methylene blue dye, *Res. Chem. Intermed.*, 43 (2017) 2669–2690.

- [6] A.A. Alqadami, M. Naushad, M.A. Abdalla, M.R. Khan, Z.A. Alothman, Adsorptive removal of toxic dye using Fe<sub>3</sub>O<sub>4</sub>-TSC nanocomposite: equilibrium, kinetic, and thermodynamic studies, *J. Chem. Eng. Data*, 61 (2016) 3806–3813.
- [7] M. Naushad, Z.A. Alothman, M.R. Awual, S.M. Alfadul, T. Ahamad, Adsorption of rose Bengal dye from aqueous solution by amberlite Ira-938 resin: kinetics, isotherms, and thermodynamic studies, *Desal. Wat. Treat.*, 57 (2016) 13527–13533.
- [8] A.B. Albadarin, M.N. Collins, M. Naushad, S. Shirazian, G. Walker, C. Mangwandi, Activated lignin-chitosan extruded blends for efficient adsorption of methylene blue, *Chem. Eng. J.*, 307 (2017) 264–272.
- [9] C. Hu, Y.Z. Wang, Decolorization and biodegradability of photocatalytic treated azo dyes and wool textile wastewater, *Chemosphere*, 39 (1999) 2107–2115.
- [10] J. Kiwi, C. Pulgarin, P. Peringer, M. Gratzel, Beneficial effects of homogeneous photo Fenton pretreatment upon the biodegradation of anthraquinone sulfonate in waste water treatment, *Appl. Catal., B*, 3 (1993) 85–99.
- [11] M. Muthukumar, N. Selvakumar, Studies on the effect of inorganic salts on decolouration of acid dye effluents by ozonation, *Dyes Pigm.*, 62 (2004) 221–228.
- [12] R.X. Yuan, S.N. Ramjaun, Z.H. Wang, J.S. Liu, Effects of chloride ion on degradation of Acid Orange 7 by sulfate radical-based advanced oxidation process: implications for formation of chlorinated aromatic compounds, *J. Hazard. Mater.*, 196 (2011) 173–179.
- [13] K. Wang, Y. Hsieh, C. Wu, C. Chang, The pH and anion effects on the heterogeneous photocatalytic degradation of o-methylbenzoic acid in TiO<sub>2</sub> aqueous suspension, *Chemosphere*, 40 (1999) 389–394.
- [14] C. Guillard, H. Lachheb, A. Houas, M. Ksibi, E. Elaloui, J.M. Herrmann, Influence of chemical structure of dyes, of pH and of inorganic salts on their photocatalytic degradation by TiO<sub>2</sub>, comparison of the efficiency of powder and supported TiO<sub>2</sub>, *J. Photochem. Photobiol., A*, 158 (2003) 27–36.
- [15] G.A. Epling, C. Lin, Investigation of retardation effects on the titanium dioxide photodegradation system, *Chemosphere*, 46 (2002) 937–944.
- [16] M. Sökmen, A. Özkan, Decolourising textile wastewater with modified titania: the effects of inorganic anions on the photocatalysis, *J. Photochem. Photobiol., A*, 147 (2002) 77–81.
- [17] K. Wang, J. Zhang, L. Lou, S. Yang, Y. Chen, UV or visible light induced photodegradation of AO7 on TiO<sub>2</sub> particles: the influence of inorganic anions, *J. Photochem. Photobiol., A*, 165 (2004) 201–207.
- [18] K.S. Novoselov, A.K. Geim, S.V. Morozov, D. Jiang, Y. Zhang, S.V. Dubonos, I.V. Grigorieva, A.A. Firsov, Electric field effect in atomically thin carbon films, *Science*, 306 (2004) 666–669.
- [19] A.K. Geim, K.S. Novoselov, The rise of graphene, *Nat. Mater.*, 6 (2007) 183–191.
- [20] M.J. Allen, V.C. Tung, R.B. Kaner, Honeycomb carbon: a review of graphene, *Chem. Rev.*, 110 (2010) 132–145.
- [21] I.V. Lightcap, T.H. Kosel, P.V. Kamat, Anchoring semiconductor and metal nanoparticles on a two-dimensional catalyst mat. Storing and shuttling electrons with reduced graphene oxide, *Nano Lett.*, 10 (2010) 577–583.
- [22] Y. Gao, D. Ma, C. Wang, J. Guan, X. Bao, Reduced graphene oxide as a catalyst for hydrogenation of nitrobenzene at room temperature, *Chem. Comm.*, 47 (2011) 2432–2434.
- [23] D. Du, P. Li, J. Ouyang, Nitrogen-doped reduced graphene oxide prepared by simultaneous thermal reduction and nitrogen doping of graphene oxide in air and its application as an electrocatalyst, *ACS Appl. Mater. Interfaces*, 7 (2015) 26952–26958.
- [24] Q. Yang, P. Siu-Kwong, Y. Kam-Chuen, Electrochemically reduced graphene oxide/carbon nanotubes composites as binder-free supercapacitor electrode, *J. Power Sources*, 311 (2016) 144–152.
- [25] S.D. Perera, R.G. Mariano, V. Khiem, N. Nijem, S. Oliver, C. Yves, K.J. Balkus, Hydrothermal synthesis of graphene-TiO<sub>2</sub> nanotube composites with enhanced photocatalytic activity, *ACS Catal.*, 2 (2012) 949–956.
- [26] N.R. Khalid, E. Ahmed, Z.L. Hong, L. Sana, M. Ahmed, Enhanced photocatalytic activity of graphene-TiO<sub>2</sub> composite under visible light irradiation, *Curr. Appl. Phys.*, 13 (2013) 659–663.
- [27] H. Zhang, X. Lv, Y. Li, Y. Wang, J. Li, P25-Graphene composite as a high performance photocatalyst, *ACS Nano*, 4 (2010) 381–385.
- [28] S. Min, G. Lu, Dye-sensitized reduced graphene oxide photocatalysts for highly efficient visible-light-driven water reduction, *J. Phys. Chem. C*, 115 (2011) 13938–13945.
- [29] K. Szymański, A.W. Morawski, S. Mozia, Humic acids removal in a photocatalytic membrane reactor with a ceramic UF membrane, *Chem. Eng. J.*, 305 (2016) 19–27.
- [30] W.S. Hummers, R.E. Offeman, Preparation of graphitic oxide, *J. Am. Chem. Soc.*, 80 (1958) 1339–1339.
- [31] Y. Wang, M. Li, H. Tang, J. Lu, J.H. Li, Application of graphene-modified electrode for selective detection of dopamine, *Electrochem. Commun.*, 11 (2009) 889–892.
- [32] C. Nethravathi, M. Rajamathi, Chemically modified graphene sheets produced by the solvothermal reduction of colloidal dispersions of graphite oxide, *Carbon*, 46 (2008) 1994–1998.
- [33] S. Stankovich, D.A. Dikin, R.D. Piner, K.A. Kohlhaas, A. Kleinhammes, Y. Jia, Y. Wu, S.T. Nguyen, R.S. Ruoff, Synthesis of graphene-based nanosheets via chemical reduction of exfoliated graphite oxide, *Carbon*, 45 (2007) 1558–1565.
- [34] A. Lerf, H. He, M. Forster, J. Klinowski, Structure of graphite oxide revisited, *J. Phys. Chem. B*, 102 (1998) 4477–4482.
- [35] G. Wang, Z. Yang, X. Li, C. Li, Synthesis of poly(aniline-co-oanisidine)-intercalated graphite oxide composite by delamination/reassembling method, *Carbon*, 43 (2005) 2564–2570.
- [36] S. Stankovich, D.A. Dikin, G.H.B. Dommett, K.M. Kohlhaas, E.J. Zimney, E.A. Stach, R.D. Piner, S.T. Nguyen, R.S. Ruoff, Graphene-based composite materials, *Nature*, 442 (2006) 282–286.
- [37] H.Y. Chen, O. Zahraa, M. Bouchy, Inhibition of the adsorption and photocatalytic degradation of an organic contaminant in an aqueous suspension of TiO<sub>2</sub> by inorganic ions, *J. Photochem. Photobiol., A*, 108 (1997) 37–44.
- [38] R. Yuan, S.N. Ramjaun, Z. Wang, J. Liu, Photocatalytic degradation and chlorination of azo dye in saline wastewater: kinetics and AOX formation, *Chem. Eng. J.*, 192 (2012) 171–178.
- [39] P.S. Yap, T.T. Lim, Effect of aqueous matrix species on synergistic removal of bisphenol-A under solar irradiation using nitrogen-doped TiO<sub>2</sub>/AC composite, *Appl. Catal., B*, 101 (2011) 709–717.
- [40] A. Rincón, C. Pulgarin, Effect of pH, inorganic ions, organic matter and H<sub>2</sub>O<sub>2</sub> on *E. coli* K12 photocatalytic inactivation by TiO<sub>2</sub>; implications in solar water disinfection, *Appl. Catal., B*, 51 (2004) 283–302.
- [41] C. Steelink, What is humic acid, *J. Chem. Educ.*, 40 (1963) 379–384.
- [42] Z. Niu, T. Ohnuki, E. Simoni, Q. Jin, Z. Chen, W. Wu, Z. Guo, Effects of dissolved and fixed humic acid on Eu(III)/Yb(III) adsorption on aluminum hydroxide: a batch and spectroscopic study, *Chem. Eng. J.*, 351 (2018) 203–209.
- [43] J.P. Aguer, C. Richard, Effect of light on humic substances: production of reactive species, *Analysis*, 27 (1999) 387–390.

## Supplementary material

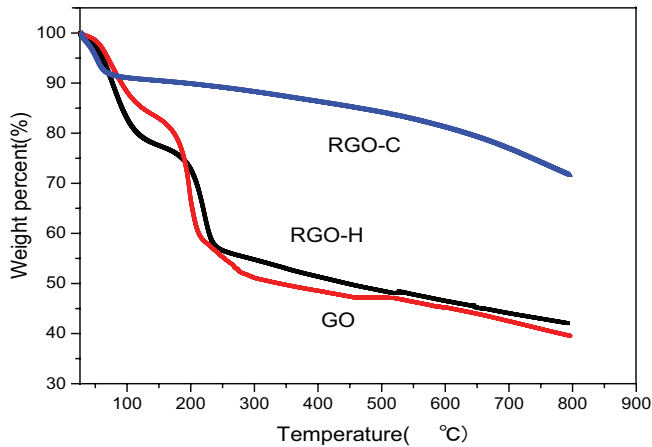


Fig. S1. TGA analysis of GO, RGO-H, and RGO-C.

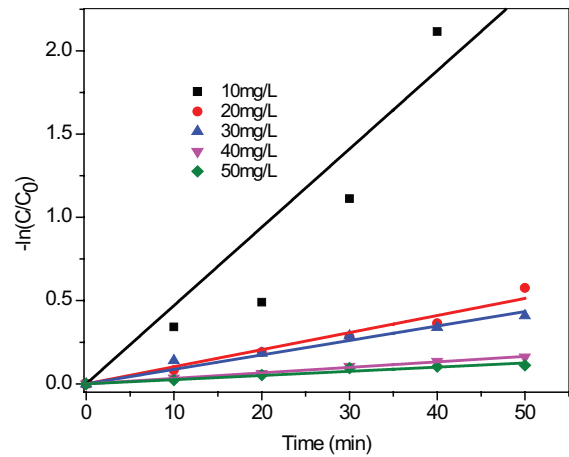
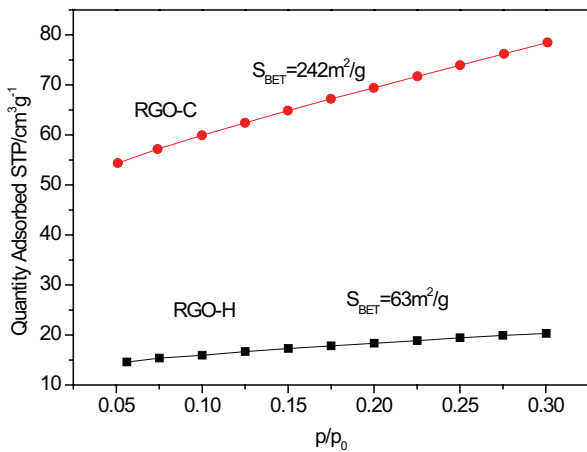
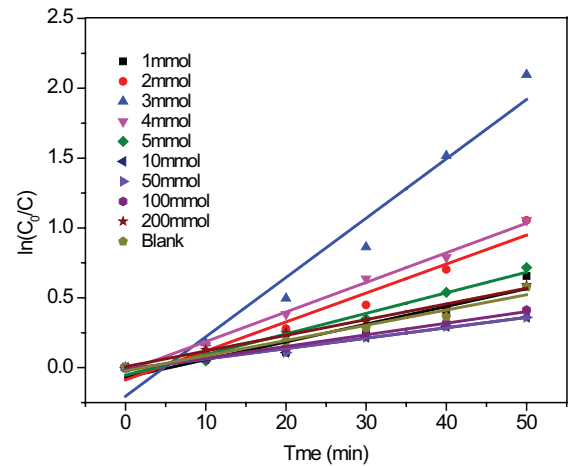
Fig. S3. The semi-logarithmic graph of  $(C/C_0)$  as a function of a time under different MB concentration.

Fig. S2. Nitrogen adsorption isotherms of RGO-H and RGO-C.

Table S1  
Degradation rate constants of MB with different concentration by RGO-H photocatalyst

MB concentration (mg L <sup>-1</sup> )	C <sub>0</sub> (mg L <sup>-1</sup> )	k (10 <sup>-2</sup> ·min <sup>-1</sup> )	R <sup>2</sup>
10	1.58	4.70	0.9617
20	5.88	1.03	0.9847
30	16.02	0.87	0.9872
40	26.83	0.33	0.9983
50	35.73	0.25	0.9805

Fig. S4. The semi-logarithmic graph of  $(C/C_0)$  as a function of a time under different Cl<sup>-</sup> concentration.